tion from the second 2+ level to the first 2+ level to be mainly $E2$, whereas the experimental finding is $M1$. It should be kept in mind that the vibrational model was proposed mainly for other regions of the periodic system.

The results of this investigation are in essential agreement with the decay schemes presented by Krisiuk *et al.*,[2] Sergeev *et al.*,[4] Emery and Kane,[20] and Hauser and Kerler.[21] The observation of a 1.800-Mev gamma ray in Po^{212} and hence the 2+ assignment for the 1.800-Mev level, however, is in disagreement with the 0+ assignment of Emery and Kane[20] and Martin and Parry.[22]

The 0.3596 ± 0.0006, $\alpha/(\alpha+\beta)$ branching ratio of Bi^{212} determined in this investigation is somewhat larger than the 0.354 ± 0.004 value[23] used by Emery and Kane.[20] It is in good agreement only with the 0.362 ± 0.006 value reported by Senftle *et al.*[24] and is larger than all other values reported, beginning with the original determination by Marsden and Barratt[25] and including the work by Prosperi and Sciuti.[26]

ACKNOWLEDGMENTS

Thanks are due to Dr. B. C. Carlson for helpful theoretical discussions, to Barry McDaniel for his assistance in evaluation of the data, to Emery and Kane,[20] and to Hauser and Kerler[21] for making their results available to us prior to publication.

[20] G. T. Emery and W. R. Kane, Phys. Rev. **118**, 755 (1960).
[21] U. Hauser and W. Kerler, Z. Physik (to be published).
[22] D. G. E. Martin and G. Parry, Proc. Phys. Soc. (London) **A68**, 1177 (1955).
[23] P. Marin, G. R. Bishop, and H. Halban, Proc. Phys. Soc. (London) **A66**, 608 (1953).
[24] F. E. Senftle, T. A. Farley, and N. Lazar, Phys. Rev. **104**, 1629 (1956).
[25] E. Marsden and T. Barratt, Proc. Phys. Soc. (London) **24**, 50 (1911).
[26] D. Prosperi and S. Sciuti, Nuovo cimento **9**, 734 (1958).

PHYSICAL REVIEW VOLUME 120, NUMBER 1 OCTOBER 1, 1960

Angular Distribution of Fragments in Fission Induced by Mev Neutrons

J. E. SIMMONS AND R. L. HENKEL*
Los Alamos Scientific Laboratory, University of California, Los Alamos, New Mexico
(Received April 1, 1960)

A multiangle gas-filled counter has been used to measure the fragment angular distribution in fission induced by neutrons in the energy range $0.5 \leq E_N \leq 9$ Mev. The target nuclei used were: Th^{230}, U^{233}, U^{234}, U^{235}, U^{236}, U^{238}, Np^{237}, and Pu^{239}. In the cases of U^{233} and U^{235} the neutron energy range was extended to include energies between 14.8 and 23 Mev. The general features of these data are the following: The anisotropy—(0°/90°) intensity ratio—has values between 1.1 and 1.2 depending on the target and is roughly independent of energy for E_N between 2 and 5.5 Mev. At higher energies a rise is observed such that at 7 Mev even-odd targets give values of anisotropy in the range 1.2 to 1.3 while even-even targets show greater values in the range 1.6 to 2.2. The anisotropy decreases somewhat by 9 Mev. Near thresholds for the even-even target nuclides considerable fluctuations of anisotropy are observed. The example of U^{236} at 0.85 Mev shows a new case of minimum intensity at 0°, the anisotropy being 0.64. In the energy region 2–4 Mev, the anisotropy of Pu^{239}, U^{233}, and U^{235} increases by a few percent from one to the next as the spin increases. This is contrary to simple theoretical expectations. These data have been compared to recent theoretical developments of the Bohr model as given by Griffin and by Halpern and Strutinski. The theory provides a satisfactory account of many features of the data.

I. INTRODUCTION

THE angular distribution of fragments from nuclear fission is related to the manner in which angular momentum is conserved. Hill and Wheeler[1] set forth a qualitative picture in a first attempt to explain early experiments on photofission[2] and neutron-induced fission.[3] At the 1955 Geneva Conference Bohr[4] presented a detailed model relating angular distributions of the fragments to the existence of rotational quantum states of the highly deformed nucleus at the barrier for fission. Wilets and Chase[5] have used this picture to fit an angular distribution in the fission[6] of Th^{232} induced by neutrons near the threshold. More recently Strutinski,[7] Halpern and Strutinski,[8] and Griffin[9] have presented more detailed developments of the Bohr model applicable when large numbers of quantum states are

* This work was supported by the U. S. Atomic Energy Commission.
[1] D. L. Hill and J. A. Wheeler, Phys. Rev. **89**, 1102 (1953).
[2] E. J. Winhold, P. T. Demos, and I. Halpern, Phys. Rev. **87**, 1139 (1952).
[3] J. E. Brolley, Jr., and W. C. Dickinson, Phys. Rev. **94**, 640 (1954).
[4] A. Bohr, *Proceedings of the International Conference on the Peaceful Uses of Atomic Energy, Geneva, 1955* (United Nations, New York, 1956), Vol. 2, p. 151.
[5] L. Wilets and D. M. Chase, Phys. Rev. **103**, 1296 (1956).
[6] R. L. Henkel and J. E. Brolley, Jr., Phys. Rev. **103**, 1292 (1956).
[7] V. M. Strutinski, Atomnaya Energ. **2**, 508 (1957) [translation: Soviet J. Atomic Energy **2**, 621 (1957)].
[8] I. Halpern and V. M. Strutinski, *Proceedings of the Second United Nations International Conference on the Peaceful Uses of Atomic Energy, Geneva, 1958* (United Nations, Geneva, 1958), Vol. 15, p. 408.
[9] J. J. Griffin, Phys. Rev. **116**, 107 (1959).

energetically possible as channels for fission at the barrier configuration.

We have measured the angular distributions of fragments in the fission induced by fast neutrons for a number of isotopes.[10] This work augments and extends experimental data obtained previous to this time. With new experimental apparatus designed for increased counting rates we have obtained data of sufficient accuracy to make meaningful comparisons with the theory.

II. OUTLINE OF THE THEORY

Bohr[4] has proposed a semiclassical expression for the angular distribution of fission fragments in fast neutron induced fission:

$$W(\theta) \propto \int dI \int dK\, f(I,K)[\sin^2\theta - K^2/I^2]^{-\frac{1}{2}}, \quad (1)$$

per unit solid angle. In this formula I is the total angular momentum of the system, K is the projection of I on the nuclear symmetry axis (Fig. 1), and θ is the angle between the neutron direction and the fragment direction. It is assumed that the target spin is negligible, which implies $\mathbf{I}=\mathbf{L}=$ (orbital angular momentum vector). The quantity $f(I,K)$ gives the distribution in I and K at the saddle point of the fissioning nucleus.

Halpern and Strutinski[8] and Griffin[9] have further developed the Bohr model. To facilitate comparisons with our data we will summarize below the relevant parts of these theories, which are based on Eq. (1). Both treatments assume that the fissioning nucleus has sufficient excitation that many quantum states are available to the fission process. The value of excitation energy above the fission threshold is taken to be $E_N - E_F$, where E_N is the neutron energy in Mev, and E_F is the neutron energy at the fission threshold. The distribution function $f(I,K)$ is assumed to be equal to a product to two factors: $F(K)G(I)$. The distribution in orbital angular momentum, $G(I)$, is taken to be the classical one, namely $G(I) \propto I$ for $I \leq I_{\max}$ and zero otherwise. The distribution of states of given K, $F(K)$ is assumed to depend on excitation energy and the fissioning species; it is specified in two different ways by the two theoretical developments.

Halpern and Strutinski[8] assume a Gaussian form for the distribution in K: $F(K) \propto \exp(-K^2/2K_0^2)$; using this they are able to partially integrate Eq. (1), obtaining:

$$W(\theta)/W(90) = \sin^{-3}\theta \left[\int_0^{U(\theta)} x^{\frac{1}{2}} e^{-x} I_0(x)\,dx\right] \Big/ \left[\int_0^{U(90)} x^{\frac{1}{2}} e^{-x} I_0(x)\,dx\right], \quad (2)$$

where $U(\theta) = (I_{\max}^2 \sin^2\theta)/4K_0^2$, and $I_0(x)$ is the zero-order Bessel function of imaginary argument. When $\theta = 0°$ the resulting value of the anisotropy[11] may be approximated by[8]:

$$W(0)/W(90) = 1 + \tfrac{1}{2}(I_{\max}/2K_0)^2. \quad (3)$$

These authors suggest that it is reasonable to use $I_{\max} = (5E_N)^{\frac{1}{2}}$ as a value for the maximum orbital angular momentum affecting the system. The expressions given in Eqs. (2) and (3) are functions of the single parameter, K_0, which is assumed to depend only on the excitation energy, $E_N - E_F$.

Griffin[9] assumes a linear form for the distribution in K, namely $F(K) \propto |K_{\max} - K|$ for $|K| \leq K_{\max}$, and zero otherwise. He suggests that this form of $F(K)$ should be suitable at low values of excitation energy. Equation (1) can again be integrated, obtaining:

$$W(\theta)/W(90) = [\bar{K} - (3/4\pi)\bar{I}\sin\theta]/[\bar{K} - (3/4\pi)\bar{I}]. \quad (4)$$

This equation is suitable for anisotropies in the range of interest here. In Eq. (4) average values of I and K have been used instead of maximum values, that is $\bar{I} = (2/3)I_{\max}$, and $\bar{K} = (1/3)K_{\max}$. We use $I_{\max}$ = (nuclear radius) × (neutron wave number), where the nuclear radius is taken to be $1.2A^{\frac{1}{3}} \times 10^{-13}$ cm, with $A = 235$, for all isotopes investigated here. Equation (4) is again a function of the single parameter $\bar{K}$, which is assumed to depend only on the excitation energy.

It will be noticed that the anisotropy as given by Eqs. (2), (3), and (4) cannot be less than unity. That is, special cases involving preferential emission of fragments at 90° for example, cannot be accommodated within this framework.

Values of anisotropy given by Eqs. (2), (3), and (4) depend on the average value of (I/K)—the larger this ratio the larger the anisotropy. When fissions occur at small excitation but at large values of neutron energy large anisotropy may be expected.[9] This situation is realized at neutron energies near 6 Mev where fission begins to occur after neutron emission, the $(n,n'f)$ process. Experimentally the anisotropy always increases at the onset of $(n,n'f)$ fission. The magnitude of the increase depends mainly on the proportion of "second chance" fissions contributing to the total fission cross section.

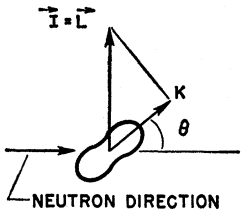

FIG. 1. Relation between I, K, and θ.

[10] Preliminary reports of these results have been presented in: Bull. Am. Phys. Soc. 4, 233, 373 (1959).

[11] The word anisotropy is defined to mean the ratio of fragment intensity per unit solid angle at zero degrees to the intensity at ninety degrees, $W(0°)/W(90°)$.

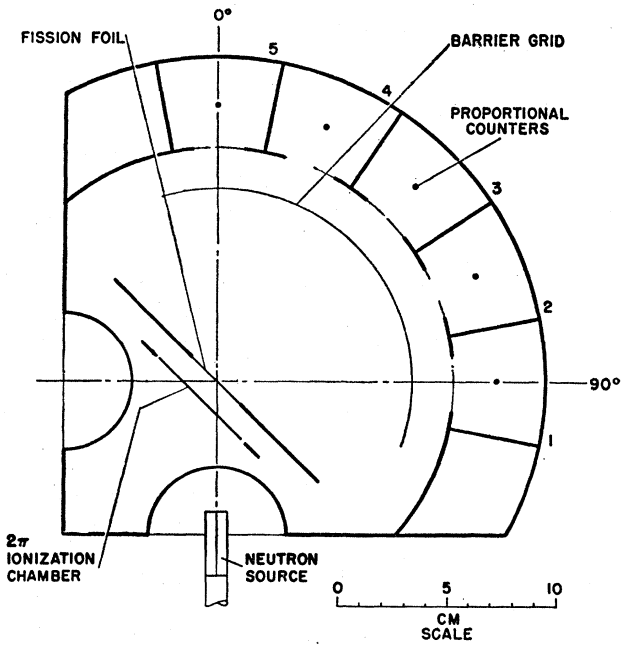

FIG. 2. Schematic drawing of the fission chamber and neutron source. The proportional counters are labeled No. 1 through 5, while the ionization counter is labeled "2π." The fission foil is fastened to a wheel foil changer with five positions.

When the target possesses spin then the total angular momentum, **I**, is the vector sum of orbital plus spin angular momentum. The direction of **I** becomes dis-oriented with respect to the incoming orbital angular momentum. Bohr[4] has pointed out that under these circumstances the fragment anisotropy should be reduced, compared to the spin zero case.

III. EXPERIMENTAL TECHNIQUE

The experimental arrangement is shown in Fig. 2. A gas-filled chamber, maintained at low pressure, is placed near a source of neutrons. Fission fragments originating in a foil are detected in five proportional ionization counters located within the chamber. The counting rates in the five counters determine the relative angular distribution of the fragments.

A. Neutron Source and Fission Foils

The experiments described here were performed at the Los Alamos large Van de Graaff facility. Monoenergetic neutrons were produced by the following reactions: $T(p,n)He^3$, $D(d,n)He^3$, and $T(d,n)He^4$, which furnished neutrons in the energy ranges 0.5 to 5, 5 to 9, and 14 to 23 Mev, respectively. Tritium or deuterium gas targets[12] were used. Under favorable circumstances neutron fluxes of the order of 10^9 per sec per steradian were available in the forward direction.

The fissionable materials were prepared as thin foils in one of several ways, which may be characterized by the thickness of backing material and by the method of deposition. For all isotopes investigated, thin-backed foils were prepared. The backing material was nominally 1.3 mg/cm^2 nickel foil held in an inconel metal clamp of 1.75-inch outside diameter. The average energy loss of fission fragments in passing through nickel foil of this thickness at normal incidence was estimated to be 30 Mev. The relatively common isotopes were deposited on the nickel foil by a vacuum evaporation process. Five to 10 milligrams of uranium oxide on a one inch diameter circle represent typical conditions. The rarer isotopes, Th^{230}, U^{234}, U^{236}, were deposited on the thin nickel foil by a painting process, wherein a nitrate solution was deposited on the foil by brush, and then heat was applied to convert the nitrate to an oxide. Typical weights of the fissionable layers were six milligrams. Owing to the fragility of the thin nickel foil, heating temperatures were limited to about 350°C. Under these circumstances the resulting fissionable layers were less uniform, and fragments suffered larger energy spreads than from evaporated foils. Foils of Th^{230} and U^{236} were also prepared by a painting technique using 0.005-inch thick platinum of 2-inch diameter as the backing material. In these cases, 2 to 3 milligrams of oxide were deposited over a 1-inch diameter circle; the resulting layers of fissionable material resulted in very small energy loss to fragments.

B. Chamber Design and Operation

The chamber consists of an outer steel envelope $\frac{1}{16}$ inch thick enclosing a low pressure gas region. Figure 2 shows a schematic plan view of the main elements. On a 5-inch diameter circle centered on the fission foil are located five proportional counters, arranged with equal spacing between zero and ninety degrees to the incident beam direction. An ionization collector plate is located behind the fission foil. This arrangement allows one to impose a coincidence requirement between a fragment entering a proportional counter and its recoil partner entering the ionization region when thin-backed foils are used. The coincidence feature of the design is helpful in reducing certain backgrounds and will be examined in greater detail later.

Each proportional counter consists of a central wire —0.008-inch diameter nickel—enclosed by thin metal box, which is roughly square in shape. A one-inch square aperture opens into each proportional region, subtending a solid angle at the foil of approximately 1/20 steradian. The window is closed to ions produced between it and the fission foil by an electrical guard potential maintained by a wire surrounding the window. The wire voltage was maintained between 550 and 600 volts by batteries, for operating gas pressures in the range of 20 to 50 mm Hg absolute. The gas consisted of a mixture of argon with 10% methane; the pressure was controlled by a precision manostat. Ions released by a fragment in passing through the proportional

[12] R. Nobles, Rev. Sci. Instr. 28, 962 (1957).

region induced signals several tens of millivolts in magnitude on the wire. Signals produced by alpha particles were some fifty times smaller in magnitude.

The ionization collector plate was maintained at about 130 volts. In this region, there being no gas amplification, signals produced by fragments were only tenths of millivolts in magnitude. Such small signals required high electronic gains to be usable and not all fragments produced signals of sufficient size to be recorded. On this account, there existed a loss in counting efficiency when using coincidence operation. This was taken into account, in a manner to be explained in Sec. III D.

In the design of this experiment we have attempted to maximize counting rates, in a manner consistent with interpretation of the data. To this end the neutron source was placed as close as reasonable to the fission foil, and the solid angle of each detector was made reasonably large. This approach has led us to make detailed calculations on the effects of geometrical resolution. The results of these calculations for the resolution function $R(\theta)$ for each counter are presented in Fig. 3. The major effect of geometrical resolution on relative counting rate is caused by unequal neutron flux distribution across the fission foil. This effect is calculated to cause the counting rate in the 90° counter to be about 1.5% higher than that in the zero degree counter.

C. Electronics

The electronic apparatus used in the experiment is shown schematically in Fig. 4. The arrangement furnished two separate scalers for recording data from each proportional counter. One of these scalers could be gated by a coincidence pulse between the ionization and proportional counters. In addition, all scalers had separate and adjustable discriminators for flexibility

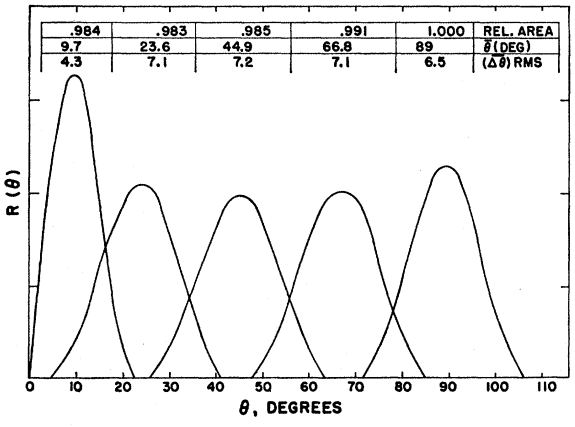

FIG. 3. Resolution functions $R(\theta)$ for the five proportional counters. $R(\theta)d\theta$ is proportional to the probability that a fragment will be detected in $d\theta$ at θ in a given counter, where isotropic fission cross section is assumed. The average values are defined by $\bar{\theta}=\int\theta R d\theta/\int R d\theta$, and $\langle(\Delta\theta)^2\rangle_{\text{av}}=\langle(\theta)^2\rangle_{\text{av}}-(\bar{\theta})^2$.

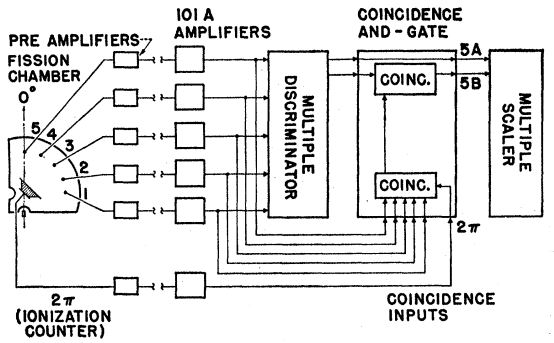

FIG. 4. Block diagram of the electronic equipment. Proportional counters 1 through 5 have similar electronic connections, but for simplicity only the connections for counter 5 is shown.

in the determination of the region of the pulse-height distribution which should be recorded. Normally the two scalers had identical discrimination levels, but only one scaler was in coincidence operation.

A 100-channel analyzer was used to obtain pulse-height distributions for use in setting discriminator levels. The stability of the electronic system was checked daily with a precision pulser, and the stability of gas amplification was checked by monitoring the pulse-height distribution of the α particles emitted from the fission foils.

D. Calibration Procedures

In the present measurements of angular distributions, efficiency correction factors were applied to the relative counting rates, which are the primary data. In some cases these efficiency factors are different from unity by only a few percent, indicating some small variation of solid angles from their design values. In other cases, owing to use of thick fission foils and coincidence operation, the relative efficiency factors differed from unity by 15%.

In the first work with this system, coincidence operation was used in the investigation of the isotopes U^{235} and U^{233}. These foils were relatively thick having evaporated layers of the oxide 1.7 and 2.0 mg/cm², respectively. Gas pressure in the counter was 40 mm Hg absolute. The relative efficiency factors were measured for each angle by utilizing the thermal fissionability of these isotopes. The counter was surrounded with about two cubic feet of paraffin, while other aspects of the geometry were maintained constant. Through a hole in the mass of paraffin the chamber was then irradiated in the usual way by neutrons of some given energy, 7 Mev for example. The increase in counting rate with paraffin in place compared to the rate without paraffin was assumed to be caused by fissions occurring isotropically in space. From the paraffin fission rate we obtained the relative counter efficiencies. During the course of the work on these isotopes we measured the efficiencies three times. It is estimated that 1% relative standard deviation is the error in each determination.

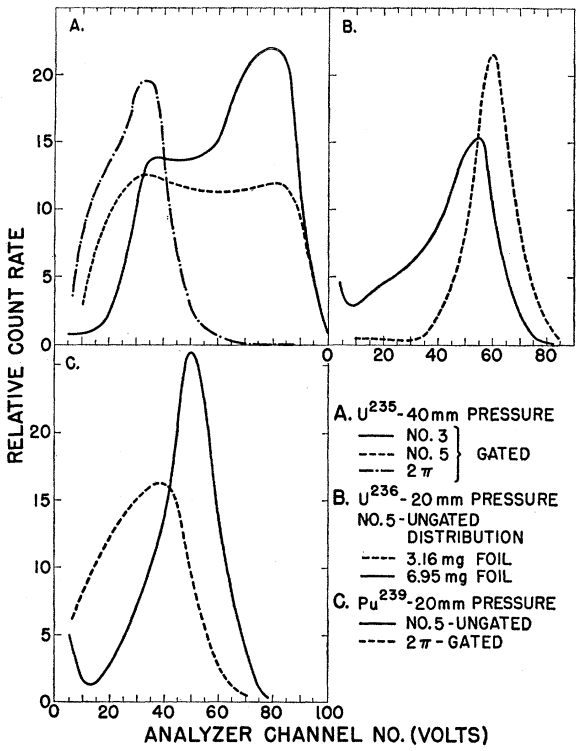

FIG. 5(A), (B), (C). Pulse-height distributions. The various counters are labeled as in Fig. 2. Gating is accomplished on the 100-channel analyzer by using the 2π-proportional counter coincidence pulse. The 2π distributions are gated by the sum of such coincidences. Figure (A) shows early work on U^{235}. In Fig. (B) the difference between thick and thin fissionable layers of U^{236} is shown. The 6.95-mg layer was painted on 1.3-mg/cm² Ni backing, while the 3.16-mg layer was painted on 0.005-inch Pt backing. Figure (C) shows distributions for a 5.53-mg foil of Pu^{239}.

The average values are listed below:

θ, degrees	90	67.5	45	22.5	0°
Relative efficiency U^{235}	1.000	1.062	1.055	1.078	1.003
Relative efficiency U^{233}	1.000	1.148	1.151	1.177	1.007

The fact that the relative efficiency is lower for the end counters is due to the fact that fragments passing through the foil at 45° lose more energy than those from the center counter. The U^{233} foil showed larger effects in this respect because of its greater thickness. In Fig. 5(A) we have plotted some typical pulse-height distributions for coincidence operation with the U^{235} isotope.

The calibration procedure described above cannot be used for isotopes which are not thermally fissile. In the measurements with the even-even isotopes and Np^{237}, the operating conditions were modified in such a way as to minimize loss of signals from fragments entering the counting volumes. The chamber gas pressure was reduced from 40 mm to 20 mm, and amplifier gain changes were made. These modifications resulted in better pulse-height distributions in the proportional counters, and allowed the use of singles counting rates with unity counter efficiency at neutron energies below 6 Mev. At neutron energies higher than 6 Mev, the coincidence requirement was used to eliminate neutron-induced background from nuclear events produced in the counter walls. The ionization (2π) counter, however, did not have unity counting efficiency with respect to fragments entering at various angles. The required relative counter efficiencies in this case were obtained by comparisons of singles and coincidence counting rates at lower neutron energies. Results obtained in this way for U^{238} agreed well with older measurements. See Sec. IV for this comparison. Comparisons of thin foil and thick foil counting rates for the isotopes U^{236} and Th^{230}, convinced us that our calibration procedures were reasonable. In Fig. 5(B) we have displayed ungated pulse-height distributions for a thick and a thin foil of U^{236}.

Measurements with Pu^{239} were also performed under these improved counter conditions. It was again possible to calibrate using the paraffin technique. The fission foil was composed of 5 mg of PuO_2 evaporated on the thin nickel backing. In Fig. 5(C) are displayed some pulse-height distributions of fission fragments for this case. One sees very little trouble from alpha particles in the proportional counter in spite of the high rate of alpha decay.

Near the end of this work a new and thinner foil (5 mg) of U^{233} was obtained. Measurements were repeated at eleven energies between two and seven Mev, and at 18 Mev, under the 20 mm pressure conditions. The anisotropies thus measured repeated the earlier work to within the limits of error.

IV. RESULTS

The results for all of our measured angular distributions are listed in Table I. In each row the neutron energy E_N is entered, followed by four columns giving values of $W(\theta)/W(90)$ which are the experimental numbers. The last column gives an extrapolation to zero degrees, $W(0)/W(90)$ obtained from a Legendre polynomial fit to the data, together with an estimate of error derived from the fit.

All of the experimental data have been fitted by a sum of Legendre polynomials of the form $\sum C_{2N}P_{2N}(\theta)$. Four terms at most were used. The curve fitting procedure was performed by the method of least squares. The method by which geometrical resolution effects were incorporated into the curve fitting procedure is outlined in the Appendix.

The value of uncertainty in energy given in Table I is equal to the half-energy loss of the incident charged particle in the gas target, for the particular neutron reaction used. Other sources of energy loss were considered to be negligible. The errors in the experimental data are standard deviations of which the major part is attributed to statistical uncertainties. The experimental data appearing in Table I have been subjected

TABLE I. Experimental values of $W(\theta)/W(90)$, as function of neutron energy.

E_N (Mev)	(67.5/90)	(45/90)	(22.5/90)	(10/90)	(0/90)-Fit
		U^{233}			
0.52±0.12	1.01±0.04	1.09±0.04	1.09±0.04	1.10±0.04	1.11±0.02
1.00±0.09	1.03±0.03	1.08±0.03	1.09±0.03	1.09±0.04	1.09±0.02
1.50±0.12	1.01±0.01	1.06±0.01	1.14±0.02	1.11±0.02	1.14±0.02
2.00±0.10	1.03±0.01	1.08±0.01	1.17±0.02	1.15±0.02	1.17±0.02
2.51±0.09	1.03±0.01	1.08±0.01	1.16±0.01	1.12±0.01	1.14±0.03
3.00±0.08	1.04±0.01	1.06±0.01	1.12±0.01	1.12±0.01	1.13±0.01
3.50±0.07	1.05±0.01	1.08±0.01	1.15±0.01	1.14±0.01	1.14±0.02
4.00±0.07	1.03±0.02	1.07±0.02	1.14±0.02	1.11±0.02	1.13±0.02
4.50±0.06	1.02±0.02	1.06±0.01	1.15±0.02	1.10±0.02	1.13±0.03
5.00±0.19	1.03±0.03	1.07±0.03	1.18±0.03	1.12±0.02	1.15±0.03
5.50±0.16	1.05±0.02	1.10±0.02	1.14±0.03	1.10±0.03	1.11±0.02
6.00±0.18	1.06±0.02	1.11±0.02	1.20±0.02	1.18±0.02	1.20±0.02
6.50±0.16	1.04±0.01	1.13±0.02	1.24±0.02	1.24±0.02	1.26±0.01
7.00±0.14	1.05±0.02	1.14±0.02	1.25±0.02	1.29±0.02	1.30±0.01
7.50±0.13	1.07±0.01	1.18±0.02	1.29±0.02	1.32±0.02	1.33±0.01
8.00±0.18	1.08±0.02	1.16±0.02	1.28±0.02	1.33±0.02	1.32±0.02
8.50±0.16	1.06±0.01	1.16±0.01	1.27±0.01	1.27±0.02	1.29±0.02
8.80±0.08	1.03±0.03	1.13±0.03	1.24±0.03	1.25±0.04	1.27±0.02
9.05±0.05	1.09±0.03	1.14±0.03	1.24±0.03	1.25±0.03	1.24±0.03
14.8 ±0.20	1.12±0.07	1.20±0.07	1.32±0.07	1.32±0.08	1.31±0.04
16.0 ±0.29	1.11±0.04	1.25±0.04	1.42±0.04	1.26±0.05	1.32±0.11
18.0 ±0.26	1.04±0.02	1.16±0.02	1.25±0.02	1.20±0.03	1.23±0.04
19.0 ±0.14	1.01±0.03	1.08±0.03	1.19±0.04	1.19±0.04	1.22±0.02
20.0 ±0.08	1.12±0.04	1.20±0.04	1.26±0.04	1.27±0.04	1.24±0.04
21.0 ±0.07	1.11±0.04	1.18±0.04	1.32±0.04	1.25±0.04	1.27±0.06
22.0 ±0.09	1.04±0.02	1.10±0.02	1.17±0.03	1.14±0.03	1.16±0.02
23.0 ±0.03	0.90±0.03	1.04±0.03	1.06±0.03	1.16±0.03	1.19±0.06
		U^{235}			
0.52±0.12	1.03±0.03	1.00±0.03	1.04±0.03	1.04±0.03	1.03±0.02
1.00±0.09	0.99±0.04	1.02±0.04	1.09±0.04	1.09±0.04	1.11±0.02
1.50±0.08	1.07±0.04	1.16±0.04	1.18±0.04	1.12±0.04	1.13±0.02
2.00±0.07	1.05±0.03	1.11±0.02	1.19±0.03	1.21±0.03	1.21±0.02
2.51±0.05	1.02±0.02	1.08±0.03	1.15±0.03	1.15±0.03	1.17±0.02
3.00±0.05	1.02±0.02	1.07±0.02	1.12±0.03	1.18±0.03	1.17±0.02
3.50±0.03	1.00±0.03	1.02±0.03	1.13±0.03	1.15±0.03	1.18±0.02
4.00±0.04	1.00±0.03	1.05±0.03	1.11±0.03	1.11±0.03	1.13±0.02
4.25±0.04	1.00±0.03	1.06±0.03	1.14±0.03	1.13±0.03	1.16±0.02
4.50±0.04	1.05±0.03	1.12±0.03	1.18±0.03	1.18±0.04	1.18±0.03
5.00±0.19	1.04±0.03	1.08±0.04	1.17±0.04	1.19±0.04	1.19±0.03
5.50±0.16	1.07±0.03	1.09±0.03	1.15±0.03	1.18±0.03	1.16±0.02
6.00±0.14	1.03±0.03	1.08±0.03	1.15±0.03	1.15±0.03	1.16±0.02
6.50±0.11	1.04±0.03	1.14±0.03	1.31±0.03	1.30±0.03	1.34±0.03
7.00±0.10	1.01±0.04	1.16±0.04	1.24±0.04	1.32±0.05	1.34±0.03
7.50±0.10	1.06±0.02	1.27±0.03	1.34±0.03	1.36±0.03	1.38±0.03
8.00±0.09	1.04±0.02	1.19±0.03	1.31±0.03	1.32±0.03	1.35±0.02
8.50±0.08	1.05±0.02	1.16±0.02	1.32±0.02	1.33±0.03	1.36±0.02
8.80±0.08	1.07±0.03	1.17±0.03	1.33±0.03	1.35±0.03	1.36±0.02
9.05±0.05	1.04±0.03	1.16±0.03	1.25±0.03	1.34±0.04	1.34±0.02
14.8 ±0.20	0.94±0.07	1.14±0.08	1.22±0.08	1.30±0.09	1.35±0.05
16.0 ±0.29	1.12±0.04	1.24±0.04	1.38±0.04	1.35±0.05	1.36±0.04
18.0 ±0.20	1.04±0.04	1.16±0.04	1.25±0.04	1.28±0.04	1.29±0.02
19.0 ±0.14	1.03±0.03	1.12±0.03	1.22±0.04	1.29±0.04	1.29±0.02
20.0 ±0.08	1.08±0.04	1.13±0.04	1.26±0.04	1.28±0.05	1.28±0.03
21.0 ±0.07	1.06±0.04	1.18±0.04	1.23±0.04	1.25±0.04	1.25±0.02
22.0 ±0.09	1.03±0.03	1.09±0.03	1.23±0.03	1.32±0.03	1.32±0.02
23.0 ±0.03	1.08±0.03	1.08±0.03	1.19±0.03	1.25±0.03	1.22±0.04
		Pu^{239}			
0.50±0.10	0.94±0.04	0.96±0.04	1.04±0.04	1.04±0.05	1.07±0.04
1.00±0.08	1.00±0.04	1.01±0.04	1.06±0.04	1.07±0.05	1.08±0.02
1.50±0.12	1.00±0.02	1.05±0.02	1.07±0.02	1.08±0.02	1.09±0.01
2.00±0.10	1.03±0.02	1.04±0.02	1.07±0.02	1.11±0.03	1.10±0.02
2.50±0.09	1.02±0.02	1.06±0.03	1.09±0.02	1.12±0.02	1.11±0.01
3.00±0.08	1.02±0.02	1.06±0.02	1.11±0.02	1.12±0.03	1.13±0.02
3.50±0.07	1.02±0.02	1.05±0.03	1.07±0.02	1.10±0.02	1.09±0.01
4.00±0.06	0.99±0.02	1.03±0.03	1.08±0.02	1.09±0.02	1.10±0.01
4.50±0.06	0.98±0.02	1.04±0.02	1.07±0.02	1.08±0.02	1.10±0.02
5.32±0.05	1.00±0.02	1.02±0.02	1.08±0.02	1.09±0.03	1.10±0.02
6.00±0.18	1.01±0.02	1.07±0.02	1.10±0.02	1.12±0.03	1.13±0.02
6.50±0.16	1.03±0.02	1.07±0.02	1.15±0.02	1.18±0.03	1.19±0.02
7.00±0.10	1.03±0.02	1.10±0.02	1.18±0.02	1.21±0.02	1.22±0.01
7.50±0.13	1.03±0.02	1.08±0.02	1.17±0.02	1.21±0.03	1.22±0.02
		Np^{237}			
1.00±0.08	1.01±0.07	1.04±0.07	1.12±0.07	1.16±0.07	1.17±0.04
1.25±0.08	1.01±0.04	1.06±0.04	1.09±0.04	1.06±0.04	1.08±0.02
1.50±0.12	1.01±0.02	1.03±0.02	1.09±0.02	1.14±0.02	1.14±0.01
1.75±0.07	0.98±0.03	1.03±0.03	1.08±0.03	1.12±0.03	1.13±0.02
2.00±0.10	0.99±0.02	1.06±0.02	1.08±0.02	1.12±0.02	1.13±0.02
2.50±0.09	1.01±0.01	1.07±0.01	1.09±0.01	1.11±0.02	1.12±0.01
3.00±0.07	0.96±0.03	1.02±0.03	1.12±0.03	1.12±0.04	1.11±0.02
3.50±0.06	1.00±0.02	1.06±0.02	1.14±0.02	1.16±0.02	1.18±0.01
4.00±0.04	1.10±0.05	1.17±0.05	1.16±0.05	1.16±0.05	1.13±0.03
4.50±0.06	0.97±0.02	0.99±0.02	1.07±0.02	1.10±0.02	1.13±0.01

E_N (Mev)	(67.5/90)	(45/90)	(22.5/90)	(10/90)	(0/90)-Fit
		Np^{237}			
5.00±0.19	1.03±0.02	1.09±0.02	1.12±0.02	1.16±0.02	1.16±0.01
5.50±0.18	1.02±0.02	1.03±0.02	1.06±0.02	1.10±0.03	1.09±0.02
6.00±0.17	1.08±0.02	1.14±0.02	1.19±0.02	1.21±0.03	1.19±0.03
6.50±0.19	1.02±0.02	1.11±0.02	1.21±0.02	1.26±0.03	1.27±0.02
7.00±0.19	1.03±0.02	1.10±0.02	1.21±0.02	1.26±0.02	1.27±0.01
7.21±0.19	1.04±0.02	1.10±0.02	1.24±0.02	1.30±0.02	1.31±0.02
7.50±0.17	1.04±0.02	1.14±0.02	1.22±0.02	1.31±0.02	1.30±0.02
8.00±0.09	1.06±0.03	1.16±0.03	1.27±0.04	1.26±0.04	1.27±0.03
8.50±0.08	1.02±0.02	1.10±0.02	1.18±0.02	1.22±0.02	1.23±0.01
8.80±0.08	1.08±0.03	1.17±0.03	1.31±0.03	1.33±0.04	1.34±0.02
		Th^{230}			
1.00±0.14	0.80±0.10	0.95±0.11	1.12±0.11	1.34±0.12	1.43±0.11
1.25±0.12	0.84±0.07	1.08±0.08	1.24±0.09	1.29±0.08	1.44±0.10
1.50±0.12	1.06±0.06	1.06±0.07	0.94±0.07	0.94±0.07	0.90±0.04
1.75±0.11	1.05±0.06	1.12±0.06	1.19±0.06	1.30±0.06	1.27±0.04
2.00±0.10	0.90±0.05	1.01±0.05	1.29±0.06	1.27±0.05	1.25±0.05
2.10±0.10	1.12±0.07	1.24±0.07	1.51±0.08	1.67±0.07	1.64±0.06
2.50±0.09	0.84±0.06	1.11±0.07	1.12±0.07	1.13±0.07	1.24±0.10
3.00±0.09	0.99±0.02	1.08±0.02	1.20±0.02	1.19±0.02	1.19±0.02
4.00±0.05	0.94±0.04	1.00±0.04	1.18±0.04	1.10±0.04	1.09±0.07
5.00±0.06	1.02±0.08	0.96±0.07	1.12±0.08	1.05±0.08	1.08±0.06
5.50±0.18	0.87±0.06	0.99±0.07	1.03±0.07	1.10±0.08	1.15±0.07
6.00±0.18	0.89±0.06	0.96±0.06	1.18±0.07	1.36±0.08	1.42±0.04
6.50±0.16	0.95±0.05	1.08±0.05	1.48±0.06	1.88±0.07	1.89±0.09
7.00±0.21	1.04±0.05	1.16±0.05	1.87±0.06	2.30±0.06	2.30±0.09
7.50±0.14	1.01±0.02	1.24±0.02	1.83±0.03	2.20±0.03	2.29±0.02
8.00±0.18	0.95±0.04	1.13±0.04	1.62±0.05	1.90±0.05	1.98±0.03
8.50±0.16	0.95±0.04	1.10±0.04	1.56±0.05	1.74±0.05	1.84±0.04
9.15±0.14	1.01±0.04	1.19±0.04	1.55±0.05	1.70±0.05	1.76±0.03
		U^{234}			
0.60±0.10	1.19±0.08	1.19±0.08	1.37±0.09	1.45±0.09	1.38±0.07
0.85±0.10	1.07±0.05	1.20±0.06	1.47±0.06	1.68±0.06	1.67±0.05
1.00±0.10	1.10±0.05	1.21±0.06	1.20±0.06	1.26±0.05	1.22±0.05
1.25±0.08	1.08±0.05	1.12±0.05	1.09±0.05	1.13±0.05	1.09±0.04
1.50±0.12	1.07±0.04	1.14±0.04	1.12±0.04	1.21±0.04	1.17±0.04
1.75±0.07	1.09±0.04	1.21±0.04	1.25±0.04	1.29±0.04	1.27±0.02
2.00±0.10	1.05±0.04	1.16±0.04	1.24±0.04	1.28±0.04	1.28±0.03
2.50±0.09	1.00±0.03	1.07±0.04	1.15±0.04	1.21±0.04	1.22±0.02
3.50±0.07	1.07±0.04	1.15±0.04	1.20±0.04	1.26±0.04	1.23±0.03
4.50±0.06	1.04±0.04	1.07±0.04	1.13±0.04	1.26±0.04	1.22±0.05
5.00±0.06	1.11±0.04	1.14±0.04	1.21±0.04	1.26±0.04	1.22±0.04
5.50±0.18	1.02±0.04	1.16±0.05	1.18±0.05	1.17±0.05	1.19±0.03
6.00±0.18	1.07±0.04	1.20±0.05	1.29±0.05	1.36±0.05	1.36±0.02
6.50±0.24	1.04±0.04	1.19±0.04	1.38±0.04	1.49±0.04	1.51±0.02
7.00±0.21	1.06±0.04	1.21±0.04	1.46±0.05	1.56±0.04	1.59±0.02
7.21±0.19	1.05±0.04	1.25±0.04	1.46±0.05	1.62±0.04	1.63±0.03
7.50±0.19	1.10±0.04	1.28±0.04	1.52±0.05	1.58±0.04	1.60±0.02
8.50±0.16	1.06±0.03	1.20±0.04	1.40±0.04	1.52±0.04	1.53±0.02
		U^{236}			
0.60±0.10	0.95±0.30	1.04±0.30	0.65±0.23	0.87±0.30	0.77±0.14
0.85±0.10	1.16±0.11	1.18±0.10	0.85±0.09	0.73±0.09	0.64±0.06
1.00±0.10	1.05±0.07	1.18±0.07	0.94±0.06	0.82±0.06	0.79±0.05
1.12±0.09	0.94±0.07	1.10±0.08	1.14±0.08	1.21±0.08	1.25±0.05
1.25±0.07	1.05±0.05	1.14±0.06	1.30±0.05	1.31±0.05	1.33±0.03
1.50±0.09	1.04±0.04	1.12±0.04	1.21±0.04	1.23±0.04	1.25±0.02
1.75±0.07	1.09±0.06	1.22±0.06	1.30±0.06	1.28±0.06	1.28±0.04
2.00±0.10	1.05±0.03	1.16±0.03	1.28±0.03	1.33±0.03	1.33±0.02
2.50±0.09	1.04±0.03	1.16±0.04	1.19±0.04	1.22±0.03	1.22±0.02
3.01±0.07	1.08±0.05	1.11±0.05	1.16±0.05	1.20±0.05	1.18±0.02
4.00±0.06	1.02±0.04	1.09±0.04	1.19±0.04	1.21±0.04	1.23±0.02
5.00±0.06	1.06±0.05	1.20±0.05	1.23±0.05	1.24±0.05	1.24±0.04
6.00±0.18	0.96±0.04	1.00±0.04	1.24±0.05	1.27±0.05	1.34±0.05
6.18±0.18	0.99±0.05	1.14±0.05	1.34±0.05	1.49±0.05	1.52±0.03
6.50±0.16	1.01±0.04	1.15±0.04	1.44±0.05	1.55±0.05	1.60±0.02
7.00±0.14	1.05±0.03	1.30±0.04	1.63±0.05	1.66±0.04	1.67±0.05
7.50±0.13	0.99±0.04	1.15±0.04	1.52±0.04	1.68±0.04	1.75±0.03
8.00±0.18	1.14±0.03	1.30±0.03	1.53±0.03	1.73±0.03	1.79±0.02
8.50±0.16	1.04±0.03	1.23±0.03	1.44±0.03	1.57±0.03	1.59±0.02
9.15±0.14	1.08±0.03	1.23±0.04	1.46±0.04	1.45±0.04	1.49±0.03
		U^{238}			
1.25±0.08	0.96±0.04	1.09±0.04	1.15±0.04	1.20±0.05	1.23±0.03
1.50±0.12	1.00±0.04	1.17±0.05	1.46±0.05	1.54±0.06	1.61±0.04
1.75±0.07	1.00±0.04	1.17±0.05	1.15±0.05	1.20±0.05	1.21±0.05
2.00±0.10	1.04±0.02	1.14±0.02	1.25±0.02	1.29±0.03	1.30±0.02
2.50±0.09	0.96±0.02	1.06±0.03	1.16±0.03	1.25±0.03	1.28±0.04
3.50±0.07	0.99±0.02	1.06±0.02	1.14±0.02	1.24±0.03	1.25±0.03
4.50±0.06	1.01±0.03	1.08±0.03	1.15±0.03	1.24±0.04	1.24±0.03
5.00±0.06	1.02±0.02	1.09±0.03	1.21±0.03	1.20±0.03	1.23±0.02
5.50±0.18	0.98±0.03	1.09±0.03	1.17±0.04	1.19±0.04	1.23±0.02
6.00±0.18	1.02±0.03	1.20±0.03	1.34±0.03	1.53±0.04	1.53±0.06
6.50±0.24	1.07±0.03	1.26±0.03	1.52±0.04	1.79±0.05	1.87±0.07
7.00±0.21	1.03±0.02	1.16±0.02	1.49±0.02	1.71±0.03	1.77±0.02
7.20±0.19	0.97±0.02	1.14±0.02	1.43±0.03	1.70±0.04	1.73±0.06
7.50±0.19	1.03±0.02	1.16±0.02	1.44±0.02	1.64±0.03	1.70±0.02
8.50±0.16	1.00±0.02	1.17±0.02	1.37±0.02	1.55±0.03	1.58±0.04

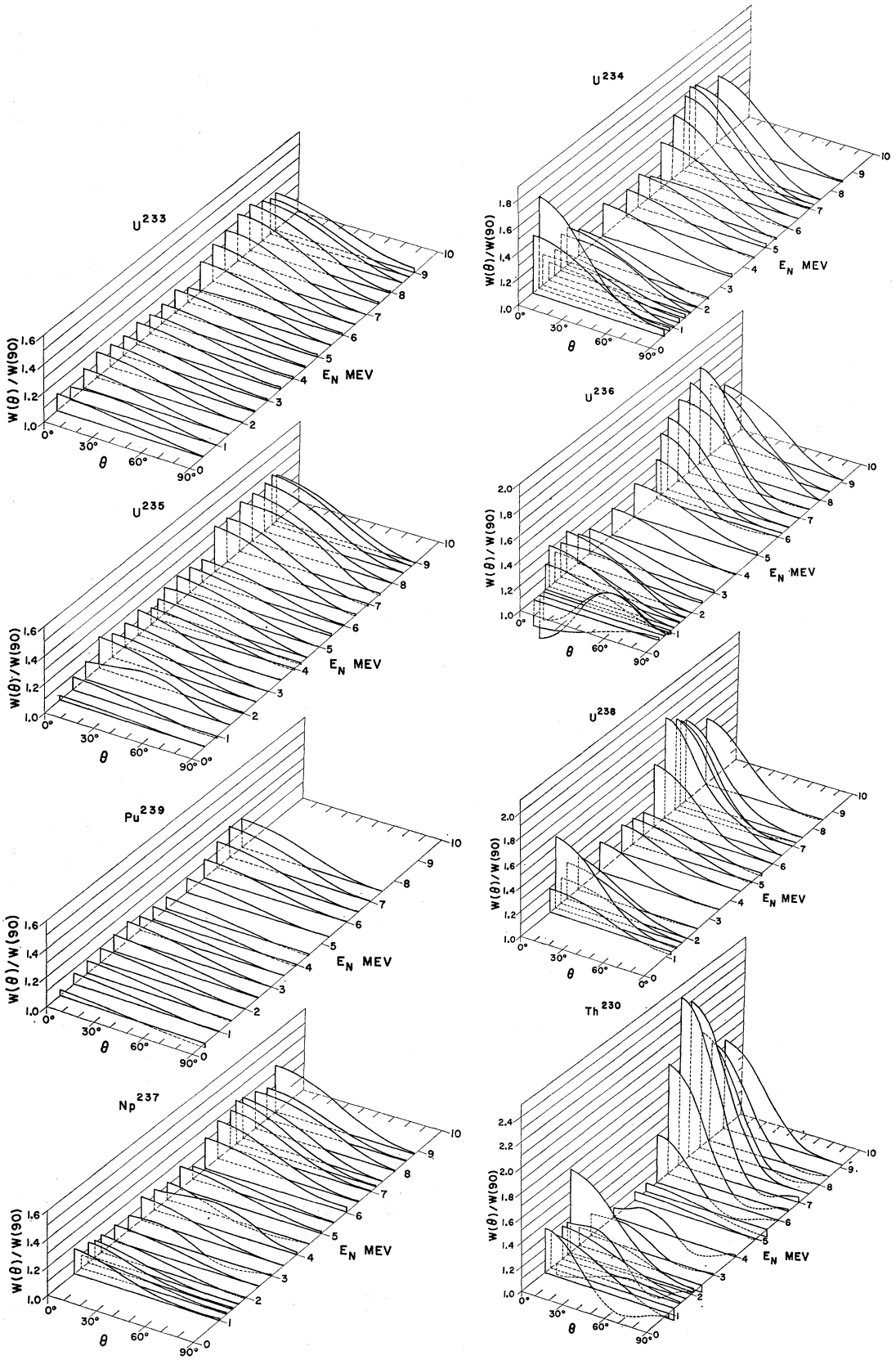
U233
U234
U235
U236
U238
Pu239
Th230
Np237
W(θ)/W(90)
θ
E_N MEV

to certain corrections. The magnitudes of these corrections are listed below:

Neutron background	1%
Accidental coincidence background	2%
Relative counter efficiency	2–15%
Break-up neutrons (E_N>21 Mev)	1%
Center-of-mass effect	1.5%
Resolution effect	2%

The uncertainties in the first three corrections were incorporated into the errors quoted with the data. The uncertainties of the last three corrections were considered to be negligible. The accidental coincidence background was included only on the early work of U^{235} and U^{233}. Corrections due to isotopic impurities have not been applied; however the magnitude of the effect is appreciable in a few cases only. In particular, the anisotropy of U^{235} is about 1% high in the energy region 6 to 9 Mev because of the presence of 6% of U^{238} and U^{234}. The Pu^{239} foil presents a similar situation on account of 5% impurity of Pu^{240}.

The error included in the column $W(0)/W(90)$-fit is often smaller than that estimated for the experimental number $W(10)/W(90)$. This is not unreasonable since the fit is a kind of average of four experimental intensity ratios whereas $W(10)/W(90)$ is of course a single such measurement. In the following pages where $W(0)/W(90)$ is graphically displayed, the errors used are the standard deviations from the fit.

In order to summarize graphically the trend of the angular distributions in the energy range 0.5 to 9 Mev, perspective three-dimensional drawings have been constructed. These are presented in Fig. 6. For each isotope the angular distributions as given by the Legendre polynomial fits to the data are plotted as a function of neutron energy. It should be noted that these Legendre expressions were not forced to give value unity at 90 degrees and were not re-normalized for Fig. 6. In the following paragraphs we shall point out in some detail the general features of the anisotropy as function of energy.

A. Odd-Mass Target Isotopes

The anisotropies of U^{233}, U^{235}, Pu^{239}, and Np^{237} derived from the Legendre polynomial fits are plotted as function of neutron energy in Fig. 7. For the sake of uniformity the energy range is restricted to the interval 0.5 to 9 Mev. Data for U^{233} and U^{235} at the higher energies between 14.8 and 23 Mev are shown in Fig. 12 where comparisons with other experiments are made.

The general features portrayed in Fig. 7 are the following: The anisotropies are roughly constant at

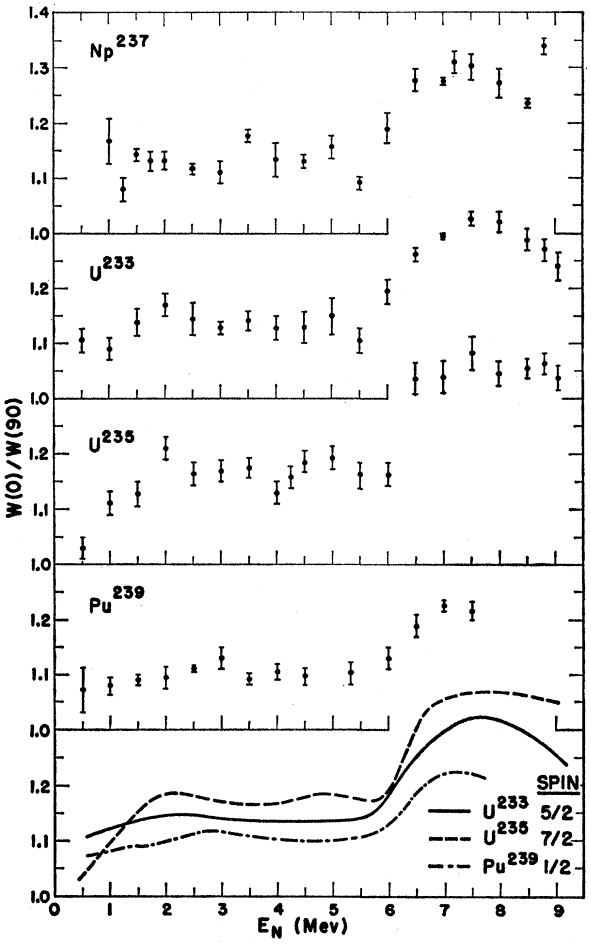

FIG. 7. $W(0)/W(90)$ versus neutron energy for Np^{237}, U^{233}, U^{235}, and Pu^{239} target nuclei. A combined display for the last three isotopes is shown at the bottom of the figure using smoothed curves through the data. These curves indicate that larger anisotropies are associated with larger spin, contrary to theoretical expectations. The errors are standard deviations as derived from the Legendre polynomial fit.

values between 1.1 and 1.2 for $E_N \leq 5.5$ Mev. The anisotropies then show an increase reaching values near 1.3 at 7.5 Mev for the uranium and neptunium isotopes; the plutonium isotope rises only to about 1.2 at this energy. The data of U^{233} show a decrease in anisotropy from 7.5 Mev to 9 Mev, which is not observed in U^{235} and Np^{237}. However, for Pu^{239} we do not have data above 7.5 Mev.

According to Bohr's suggestion concerning the effect of target spin the anisotropy of Pu^{239} (spin $\frac{1}{2}$) should be greater than that of U^{233} (spin $\frac{5}{2}$). Comparison with U^{235} (spin $\frac{7}{2}$) is not direct since the excitation at given neutron energy is about 1.0 Mev less (see Table V). At the bottom of Fig. 7 are smoothed curves comparing the anisotropies for U^{233}, U^{235}, and Pu^{239}. It will be seen

FIG. 6. Perspective drawings of the relative angular distribution of fission fragments. The curves, labeled according to target nucleus, represent the Legendre polynomial fits to the data. They have not been re-normalized to value unity at 90 degrees in spite of the label $W(\theta)/W(90)$.

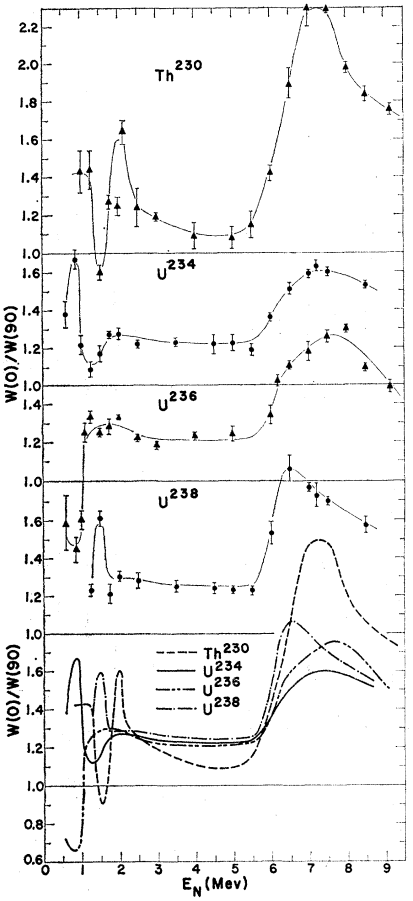

FIG. 8. $W(0)/W(90)$ versus neutron energy for Th^{230}, U^{234}, U^{236}, and U^{238} target nuclei. A combined display is shown at the bottom using smoothed curves through the data. The errors are standard deviations derived from the Legendre polynomial fit.

that for these three nuclei the larger values of anisotropy are associated with larger values of spin. To put these observations in more quantitative terms we average the experimental values $W(10)/W(90)$ in the neutron energy range below 4 Mev. When we compare these average values for the three nuclei, the following ratios are obtained: $(U^{233})/(Pu^{239})=1.02$, and $(U^{235})/(U^{233})=1.02$. The same result would have been obtained for averages of $W(0)/W(90)$. The data are not in accord with Bohr's suggestion concerning the spin effect.

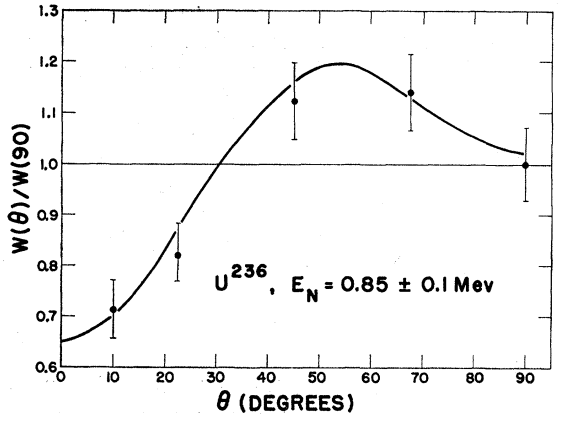

FIG. 9. Angular distribution of fragments from U^{236} target nucleus at $E_N=0.85$ Mev. A tendency toward sideways peaking is illustrated.

B. Even-Mass Target Isotopes

The anisotropies of Th^{230}, U^{234}, U^{236}, and U^{238} derived from Legendre polynomial fits are plotted as function of neutron energy in Fig. 8. Comparisons with other experiments are made in a later paragraph. The anisotropies from even mass targets are qualitatively similar to the odd mass data at neutron energies above 2 Mev. However the rise in anisotropy above 5.5 Mev is considerably steeper for the even mass targets and higher values of anisotropy are attained between 6 and 8 Mev. For example the anisotropy for Th^{230} at $E_N=7$ Mev is equal to 2.3; and the anisotropy for U^{238} at the same energy is about 1.6.

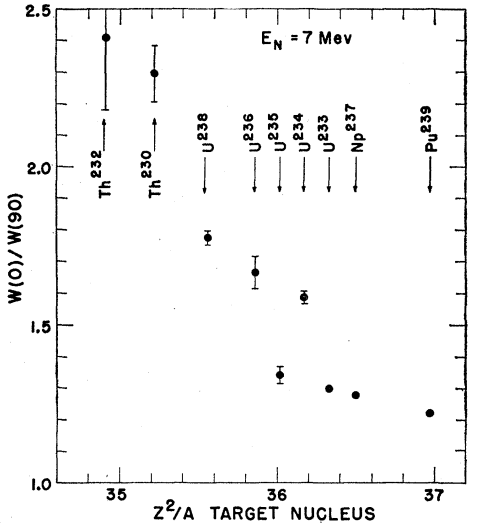

FIG. 10. Anisotropy as function of Z^2/A of the target nucleus at $E_N=7.0$ Mev. The value for Th^{232} is from reference 6.

For values of excitation energy less than one Mev, it is possible that fission can occur through a limited number of levels of the deformed nucleus. Such conditions can give rise to large fluctuations in the anisotropy not covered by the essentially statistical theories of fission anisotropy. An outstanding case of this type is already known,[6] that of Th^{232} at $E_N=1.60$ Mev. The angular distribution shows a very pronounced dip in intensity at 0° compared to 90°. This case was analyzed by Wilets and Chase,[5] by assuming that the fission occurred through the three lowest members of a $K=\frac{3}{2}$ rotational band, plus an isotropic component.

In the present work with positive-threshold even-even target isotopes, we have found an additional case of sidewise peaking in the angular distribution, namely

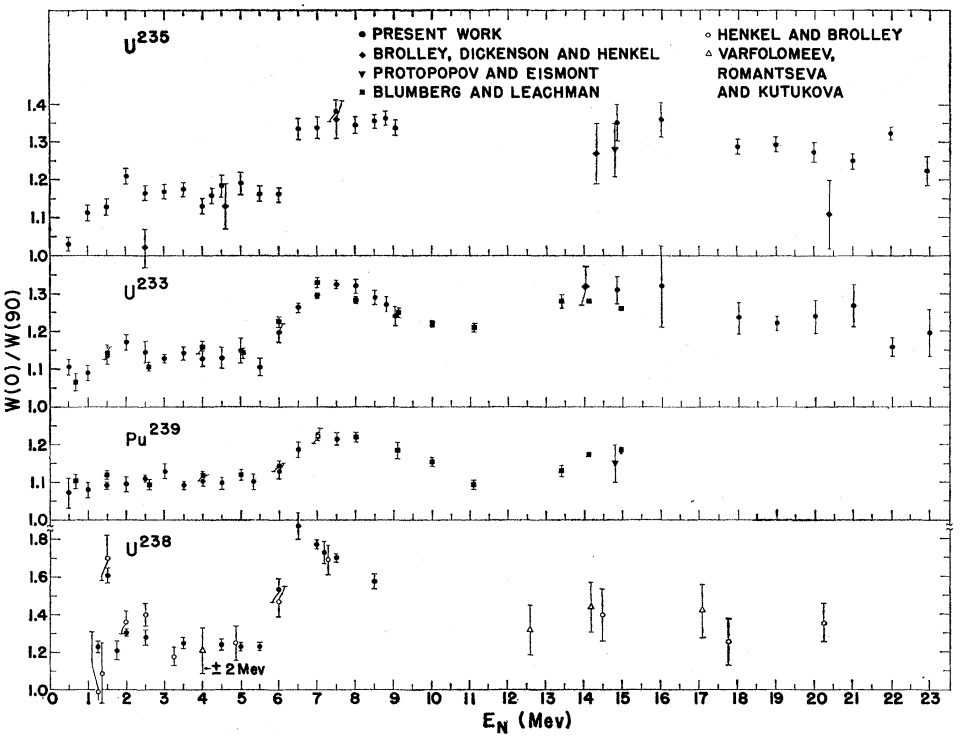

FIG. 11. Comparisons with other experiments. Anisotropies as function of neutron energy are compared for the target nuclei U^{235}, U^{233}, Pu^{239}, and U^{238}. Note the reduced scale of ordinates for U^{238}. References are given in the text.

that of U^{236} at neutron energies of 0.6, 0.85, and 1.0 Mev. The effect is most marked at $E_N=0.85$ Mev; this angular distribution is displayed in Fig. 9. It will be noted that while the angular distribution attempts to rise from 90°, it turns over near 50° and falls to a value of $W(0)/W(90)=0.64\pm0.06$ at 0°. There may be a similar case for Th^{230} at $E_N=1.50$ Mev.

Concerning the data for Th^{230} there seems to be a discrepancy at $E_N=2.0$ and 2.1 Mev. A study of the data suggests an error in energy in either or both of these data points.

C. Correlation with Z^2/A

In Fig. 10 are plotted values of the anisotropy $W(0)/W(90)$ as function of Z^2/A of the target nucleus at $E_N=7$ Mev. A definite trend is present; anisotropy decreases as Z^2/A increases. This behavior is in accord with theoretical expectations in which smaller cross sections from $(n,n'f)$ processes are expected as Z^2/A increases. The question of deviations from this trend because of possible competition between the $(n,n'f)$ and $(n,2n')$ processes will be discussed in Sec. V.

D. Comparisons with Other Experiments

Concerning U^{235}, the present investigation has changed the values of anisotropy below 2.5 Mev which were suggested by the previous experiments. The relevant data[13] are shown in Fig. 11. The prior point at $E_N=2.5$ Mev gave the impression of isotropy at this energy. The present measurements show that the neutron energy must be reduced to 0.5 Mev or below in order to obtain near-isotropy in the angular distribution.

There has been recent work at Los Alamos on the isotopes U^{233} and Pu^{239} by Blumberg and Leachman[14,15] and their collaborators. These authors used a catcher technique combined with fissionable layers thick compared to the range of fission fragments and they obtained information at energies between 0.6 and 15 Mev. There are also data on the anisotropy[3,16] of Pu^{239} and U^{233} near 14 Mev. The data on U^{233} and Pu^{239} are displayed in Fig. 11. Certain data[17] on Pu^{239} obtained by the present authors with a collimator-ionization chamber have not been included because of their large statistical uncertainties. It is seen that there is reasonable agreement between the various data.

In regard to the isotope U^{238} there is generally good agreement between the data presented here and that of previous investigators.[6,18] At values of E_N lower than

[13] J. E. Brolley, W. C. Dickinson, and R. L. Henkel, Phys. Rev. **99**, 159 (1955).

[14] L. Blumberg, J. Bahcall, D. Garrett, and R. B. Leachman, Bull. Am. Phys. Soc. **4**, 31 (1959).

[15] L. Blumberg and R. B. Leachman, Phys. Rev. **116**, 102 (1959).

[16] A. N. Protopopov and V. P. Eismont [translation: Soviet Phys.—J. Exptl. Theoret. Phys. (U.S.S.R) **34**, 250 (1958)], JETP **34(7)**, 173 (1958).

[17] J. E. Simmons, R. L. Henkel, and J. E. Brolley, Bull. Am. Phys. Soc. **2**, 308 (1957).

[18] A. A. Varfolomeev, A. S. Romantseva, and V. M. Kutukova, Doklady Akad. Nauk (S.S.S.R.) **105(4)**, 693 (1955), (Atomic Energy Research Establishment Library Translation No. 707, July, 1956).

9 Mev the present data have achieved somewhat greater accuracy than was previously possible. The various values of anisotropy are displayed in Fig. 11 as function of E_N.

The previous experimental work[19] on U^{234} has so far only been described in qualitative terms and covers the neutron energy range 0.4 to 4 Mev. Our data are in general agreement with the description of these results except at one energy. At $E_N=600$ kev a tendency for the fragments to prefer emission at 90 degrees was reported. We have investigated the anisotropy at the neutron energy $E_N=600\pm100$ kev and we found forward peaking $W(0)/W(90)\simeq1.4$. It is probable, however, that the sideways peaking is a sharp function of energy, and could have been masked by our large energy spread.

V. COMPARISON WITH THEORY

A. Qualitative Considerations

Concerning the spin effect, the simple form of the Bohr theory tells us to expect smaller anisotropy when the target spin, I_0, is large. Experimentally this is not observed, at least where comparisons between U^{233}, U^{235}, and Pu^{239} are involved at neutron energies of several Mev (Fig. 7). Theory does, however, provide two possible approaches to this problem. Griffin[9] has suggested that neutrons are absorbed into the cigar-shaped target nucleus in such a fashion as to favor the formation of states of large $\mathbf{I}=\mathbf{L}+\mathbf{I}_0$ and thereby to increase forward peaking when I_0 is large. His calculations indicate that this mechanism may account for part of the effect. Another approach is to consider that the neutron and fission widths may be a function of I, the magnitude of the total angular momentum of the system. Mottelson[20] has pointed out that a mechanism may exist which would cause Γ_F/Γ_N to be larger[21] for large values of I than for small ones. This possibility then allows states of large I to be favored, and thereby to increase the forward peaking in spite of the disorienting effect of the target spin.

The anisotropy as a function of neutron energy generally shows an increase near 5.5 Mev when fission after neutron emission becomes possible. This is true for all isotopes that have been studied. From experimental work[15] at 10 and 11 Mev and at 14 Mev and above on the isotopes Pu^{239} and U^{233}, there is also an indication of an increase in anisotropy near 12 Mev where fission after the emission of two neutrons becomes possible. The statistical theories,[8,9] through their dependence on excitation energy, give an explanation for these observations. This comes about, as mentioned earlier, since the nucleus that fissions subsequent to the emission of a neutron does so at lower excitation and contributes therefore higher anisotropy. In addition considerations of fissionability lead one to expect that anisotropy in the $(n,n'f)$ region (E_N in the range 6–10 Mev) decreases with increasing fissionability. We see a trend in this direction as demonstrated by Fig. 10 of Sec. IV, where anisotropy is plotted against Z^2/A of the target nucleus for neutron energy of 7 Mev.

In a number of even-even nuclei, the neutron binding energy is larger than the energy required to cause fission at the fission threshold. For these nuclei the $(n,n'f)$ process begins at a lower value of neutron energy than does the $(n,2n')$ process. There can be, therefore, an energy interval where the $(n,n'f)$ process does not have to compete with the $(n,2n')$ process. These considerations have led Griffin[9] to suggest that anisotropies should be specially large in this energy interval. He suggests that for neutron energies in the neighborhood of 7 Mev the fact that the anisotropy of Th^{232} is larger than that of U^{238} can be explained in this way. In order to examine this point more closely we list in Table II fission thresholds [equivalent to neutron energy at which $(n,n'f)$ begins] and neutron binding energies for nuclei of interest here. It is seen that Th^{230} and U^{234} have specially large differences in these quantities. When one examines the trend of anisotropy versus Z^2/A at $E_N=7.0$ Mev (Fig. 10) one does not see marked deviations from a smooth curve. Similar results are given by the examination of data at 6.5 Mev. It appears that the existence of an energy interval where the $(n,n'f)$ process is free of competition does not affect the anisotropies strongly.

B. Quantitative Considerations

In the following paragraphs are presented the results of numerical comparisons with the theory. The first approach was to fit the theoretical angular distributions to the data in order to ascertain the relative merits of the two theoretical expressions. Secondly, using Eq. (3) the parameter K_0^2 was calculated from the values of anisotropy of the various isotopes. The object here is

TABLE II. Comparison of fission thresholds and neutron binding energies.

Isotope	Fission threshold, Mev Cameron[a]	Fission threshold, Mev Estimate[b]	Neutron binding energy,[c] Mev
Th^{230}	···	5.7±0.2	6.68
Th^{232}	5.95	6.0±0.2	6.31
U^{234}	···	5.6±0.2	6.74
U^{236}	···	6.0±0.2	6.39
U^{238}	5.8	5.9±0.2	5.99

[a] A. G. W. Cameron, in Proceedings of the Symposium on Physics of Fission, Chalk River, Ontario, Canada, 1956 [Chalk River Laboratory Report CRP-642-A (unpublished)], p. 189. These values are the classical thresholds defined at 50% of the rise of the (n,f) excitation function.

[b] These thresholds were obtained from the neutron energy at which either the total fission cross section [Allen and Henkel, *Progress in Nuclear Energy*, edited by R. A. Charpie *et al.* (Pergamon Press, New York, 1958), Ser. I, Vol. 2], or the anisotropy (Fig. 9, present work) begins to increase due to the onset of the $(n,n'f)$ process.

[c] R. A. Glass, S. G. Thompson, and G. T. Seaborg, J. Inorg. & Nuclear Chem. 1, 3 (1955).

[19] R. W. Lamphere (private communication).

[20] Private communication.

[21] I. Halpern, *Annual Review of Nuclear Science* (Annual Reviews, Inc., Palo Alto, California, 1959), Vol. 9, p. 245.

to determine the worth of this single parameter in correlating the various data. For the sake of simplicity this work was undertaken at neutron energies less than 5.5 Mev where fission after neutron emission does not occur; energies near fission thresholds were avoided.

The theoretical angular distributions of Halpern and Strutinski given by Eq. (2), and that of Griffin in Eq. (4) have been fit to the experimental data by a method of least squares. This has been done for all isotopes in the energy range stated above. In Fig. 12 some examples of the results of the process are provided at $E_N=4$ Mev. A quantitative measure of the goodness-of-fit is provided by the parameter, "sigma," which is equal to: (Sum of squares of deviations)$^{\frac{1}{2}}/M^{\frac{1}{2}}$, where M is equal to the number of experimental points minus the number of coefficients or parameters used in the fit. In Table III are listed values of sigma averaged over certain groups of isotopes for the theoretical fits, and for the empirical Legendre polynomial fits described in Sec. IV. It is seen that the two different theoretical expressions fit the data equally well. However the values of sigma derived from the theoretical fits are about 50% larger than those obtained by fitting with Legendre polynomials.

We next determined to what extent the K parameter correlates the experimental value of anisotropy for different excitation energies. It is convenient to use the K_0^2 parameter, which appears in Eqs. (2) and (3).

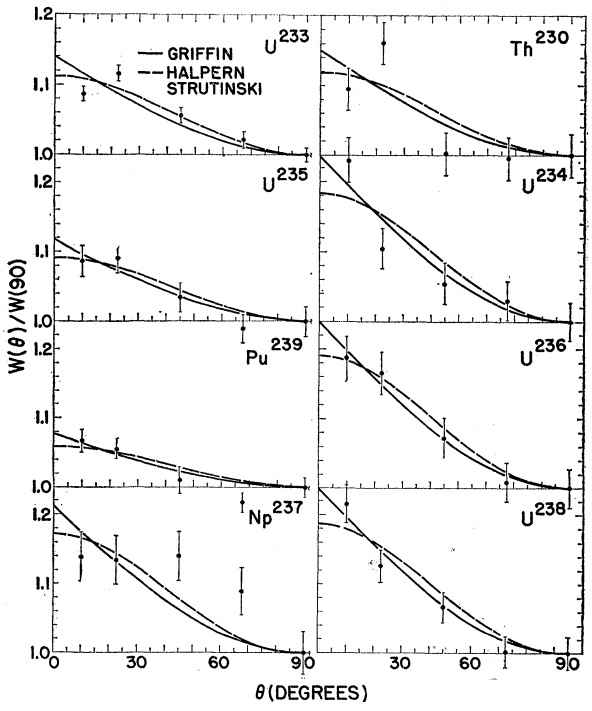

FIG. 12. Examples of theoretical fits of angular distribution to the experimental data. The neutron energy is $E_N=4$ Mev, with two exceptions: U^{234} and U^{238} which are at 4.5 Mev. The dashed curve is the fit of Halpern and Strutinski obtained from Eq. (2); the solid curve is the fit of Griffin from Eq. (4).

TABLE III. Average values of sigma.

Class of target isotopes	Equation (2) fit	Equation (4) fit	Legendre polynomial fit
Even-even	0.039	0.042	0.028
Odd	0.021	0.022	0.013
All isotopes	0.028	0.029	0.018

TABLE IV. Values of E_F[a] (neutron energy at the fission threshold) used to correlate K_0^2 with excitation energy.

Target nucleus	E_F (Mev)	Target nucleus	E_F (Mev)
Pu^{239}	−1.6	Th^{230}	0.8
U^{233}	−1.6	U^{234}	0.4
U^{235}	−0.9	U^{236}	0.8
Np^{237}	0.4	U^{238}	1.25

[a] For Pu^{239} and U^{233} values of E_F given above are approximately those of J. A. Northrop, R. H. Stokes, and K. Boyer, Phys. Rev. 115, 1277 (1959). The value for U^{235} represents approximately the energy at 10% of the peak of the excitation function given by Northrop et al. For the Np and U nuclei, fission thresholds are taken to be the energies at which the fission cross sections are 10% of the 3–5-Mev plateau. The value of E_F for Th^{230} was obtained by comparison with the uranium isotopes.

By means of Eq. (3) a value of K_0^2 was calculated for each experimental anisotropy. The resulting values of K_0^2 as function of excitation energy, E_N-E_F, were then fitted by straight lines for several classes of isotopes. The classes are arranged according to even or odd mass of the compound nuclei: (1) even-even, composed of U^{233}, U^{235}, and Pu^{239} targets, (2) even-odd, composed of U^{234}, U^{236}, and U^{238} targets, (3) odd-odd, composed of the Np^{237} target. The results of this procedure are plotted in Fig. 13. Values of E_F (neutron energy at the fission threshold) are listed in Table IV.

Several observations can be made: (1) The straight-line fits to the even-even and even-odd categories can be used to predict an unknown value of anisotropy with a 3% relative standard deviation. This number, obtained from the goodness-of-fit parameter, represents a good correlation. (2) The straight-line fits extrapolate approximately through the origin for the odd categories; however for the even-even nuclei the straight line extrapolates to zero at approximately 1-Mev excitation energy. This is compatible with the fact that even-even nuclei generally have abnormally low level density below 1 Mev compared to that of odd nuclei. (3) At low excitations the *o-o* category provides largest values of K_0^2, with smaller values being given by the *o-e* and *e-e* species respectively. At sufficiently high excitation it is expected that the value of K_0^2 would be independent of the even or odd classification of the compound nucleus. This effect may appear in the case of *e-e* and *e-o* groups where the values of K_0^2 merge at 5-Mev excitation energy.

ACKNOWLEDGMENTS

We are indebted to Mr. Blair Swartz for his work in performing calculations on counter resolution and data fitting. We wish to thank Dr. George Baker for a

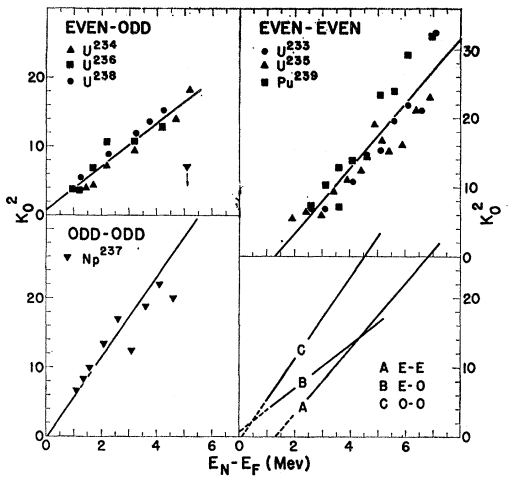

FIG. 13. The relationship between K_0^2 and excitation energy, E_N-E_F. Using Eq. (3), values of K_0^2 are calculated from the measured anisotropy for each isotope for neutron energies less than 5.5 Mev, and above thresholds. Straight-line fits of the form $K_0^2=B_1+B_2(E_N-E_F)$ have been made for three categories of compound nuclei. The categories and values of the constants B_1, B_2 and sigma (goodness-of-fit parameter) are listed below: (1) Even-odd, $B_1=0.87\pm0.76$, $B_2=3.1\pm0.25$, sigma=1.35, (2) Even-even, $B_1=-6.1\pm1.9$, $B_2=4.7\pm0.39$, sigma=3.2 (3) Odd-odd, $B_1=-0.4\pm3.6$, $B_2=5.9\pm1.1$, sigma=4.7. Sigma has been defined in the text.

helpful suggestion concerning resolution effects in the least squares analysis. We appreciate the efforts of Mr. Charles Lehman in the construction of the perspective drawings. To Mr. John Povelites we are grateful for the preparation of the many foils of fissionable material. Mrs. Dana Douglass helped greatly with Van de Graaff operation and the help of Mrs. Hope Pomeroy was valuable with data reduction. It is a pleasure to acknowledge helpful conversations with Dr. James Griffin concerning theoretical aspects of this problem.

APPENDIX: LEAST SQUARES FITS OF THE EXPERIMENTAL DATA

The experimentally measured intensities for the jth counter ($j=1, \cdots 5$) are denoted by $I(j)$. It is assumed that $W(\theta)$, the relative differential cross section of the fission fragments is given by a sum of the form, $W(\theta)=\Sigma C_{2N}P_{2N}(\theta)$, where N varies from the value zero to $N_{\max}=3$. The $P_{2N}(\theta)$ are Legendre polynomials chosen to be symmetric about ninety degrees. It is desired to find those values of the constants, C_{2N}, which provide the best fit to the measured intensities $I(j)$. Account is taken of the effects of geometrical resolution effects as follows: The intensity of the jth counter is given by

$$I(j)=\text{const}\times\int\int dA_1 dA_2[\cos(\mathbf{r}_2,\mathbf{dA}_2)W(\theta)]/[r_1^2 r_2^2].$$

In this expression dA_1 and dA_2 represent elements of area in the fission foil and in the counter aperture respectively, r_1 is the distance between neutron source and dA_1, r_2 is the distance between dA_1 and dA_2, while θ is the angle between $\mathbf{r}_1$ and $\mathbf{r}_2$. It is assumed that the distribution of neutrons from the source is isotropic in space. This assumption was justified by detailed calculations. On introducing the sum $\sum C_{2N}P_{2N}(\theta)$ in place of $W(\theta)$ we may write,

$$I(j)=\sum C_{2N}A_{2N,j}.$$

There are five such equations, one for each counter, to be solved for the best values of C_{2N}. The constants $A_{2N,j}$ are a set of known constants involving a double integral over the geometry and the known functions $P_{2N}(\theta)$. The values of the constants C_{2N} were obtained by the method of least squares for $N_{\max}$ equal to 0, 1, 2, or 3 and the best set was chosen by minimizing a goodness-of-fit parameter.